NASA/TM—2002-211476

Considerations in the Measurement of Inlet Distortion for High Cycle Fatigue in Compact Inlet Diffusers

Bernhard H. Anderson
Glenn Research Center, Cleveland, Ohio

Dennis J. Keller
RealWorld Quality Systems, Cleveland, Ohio

March 2002

The NASA STI Program Office . . . in Profile

Since its founding, NASA has been dedicated to the advancement of aeronautics and space science. The NASA Scientific and Technical Information (STI) Program Office plays a key part in helping NASA maintain this important role.

The NASA STI Program Office is operated by Langley Research Center, the Lead Center for NASA's scientific and technical information. The NASA STI Program Office provides access to the NASA STI Database, the largest collection of aeronautical and space science STI in the world. The Program Office is also NASA's institutional mechanism for disseminating the results of its research and development activities. These results are published by NASA in the NASA STI Report Series, which includes the following report types:

- TECHNICAL PUBLICATION. Reports of completed research or a major significant phase of research that present the results of NASA programs and include extensive data or theoretical analysis. Includes compilations of significant scientific and technical data and information deemed to be of continuing reference value. NASA's counterpart of peer-reviewed formal professional papers but has less stringent limitations on manuscript length and extent of graphic presentations.

- TECHNICAL MEMORANDUM. Scientific and technical findings that are preliminary or of specialized interest, e.g., quick release reports, working papers, and bibliographies that contain minimal annotation. Does not contain extensive analysis.

- CONTRACTOR REPORT. Scientific and technical findings by NASA-sponsored contractors and grantees.

- CONFERENCE PUBLICATION. Collected papers from scientific and technical conferences, symposia, seminars, or other meetings sponsored or cosponsored by NASA.

- SPECIAL PUBLICATION. Scientific, technical, or historical information from NASA programs, projects, and missions, often concerned with subjects having substantial public interest.

- TECHNICAL TRANSLATION. English-language translations of foreign scientific and technical material pertinent to NASA's mission.

Specialized services that complement the STI Program Office's diverse offerings include creating custom thesauri, building customized data bases, organizing and publishing research results . . . even providing videos.

For more information about the NASA STI Program Office, see the following:

- Access the NASA STI Program Home Page at ***http://www.sti.nasa.gov***

- E-mail your question via the Internet to help@sti.nasa.gov

- Fax your question to the NASA Access Help Desk at 301–621–0134

- Telephone the NASA Access Help Desk at 301–621–0390

- Write to:
  NASA Access Help Desk
  NASA Center for AeroSpace Information
  7121 Standard Drive
  Hanover, MD 21076

NASA/TM—2002-211476

Considerations in the Measurement of Inlet Distortion for High Cycle Fatigue in Compact Inlet Diffusers

Bernhard H. Anderson
Glenn Research Center, Cleveland, Ohio

Dennis J. Keller
RealWorld Quality Systems, Cleveland, Ohio

National Aeronautics and
Space Administration

Glenn Research Center

March 2002

Available from

NASA Center for Aerospace Information
7121 Standard Drive
Hanover, MD 21076

National Technical Information Service
5285 Port Royal Road
Springfield, VA 22100

Available electronically at http://gltrs.grc.nasa.gov/GLTRS

CONSIDERATIONS IN THE MEASUREMENT OF INLET DISTORTION FOR HIGH CYCLE FATIGUE IN COMPACT INLET DIFFUSERS

Bernhard H. Anderson
National Aeronautics and Space Administration
Glenn Research Center
Cleveland, Ohio 44135

Dennis J. Keller
RealWorld Quality Systems
Cleveland, Ohio 44116

ABSTRACT

It is the purpose of this study to examine the effects of engine face rake geometry (i.e. number of rake arms) and its use (i.e. with and without clocking) on the estimation of the first five Fourier harmonic 1/2 amplitudes of engine face distortion over a varied and significant set of cases. By combining the concepts of CFD analysis and Design of Experiments methodologies, a varied set of cases can be defined and analyzed which represent a large range of distortion patterns for a particular application. From the information gathered from this methodology, a rake geometry for use in Wind Tunnel tests can reasonably be defined which accurately measures the amplitudes at the "# per rev" frequencies of interest. Three rake arrays were considered for this study, a 40-probe, 60-probe and 80-probe array, while two methods of acquiring the data from each of these rake arrays were examined. One method of acquiring probe data was to fix each of the rake arrays in its 0° clocking angle and acquire a single set of probe data. The second approach was to clock each of the rake arrays over ten locations between the 0° clocking angle and the respective rake angle. In general, as the number of arms on the rake array increased, both random and systematic errors associated with measurement of the Fourier harmonic 1/2 amplitudes decreased. Clocking the rake and using the mean of ten clocking angles to represent the metric of interest always improved both precision and accuracy. The 40-probe rake array results probably provided random and systematic measurement errors that were too large to be of value. The 60-probe rake array used with clocking gave both very low random and systematic measurement errors up through the fourth Fourier harmonic 1/2 amplitude.The 80-probe rake with clocking provide both low random and systematic measurement errors up through the fifth Fourier harmonic 1/2 amplitude. In deciding the performance of different rake arrays to precisely and accurately provide estimates of the Fourier harmonic 1/2 amplitudes, consideration must be give as to whether clocking would be used in the data acquisition. Large reductions in both random and systematic measurement errors can be realized by clocking the engine face rake. In general, the kind of survey rake that is chosen for a Wind Tunnel experiment and the rake methodology used in providing the total pressure data needed to estimate the Fourier harmonic 1/2 amplitudes depends on the researcher's objectives and the magnitude of errors that are acceptable within the stated goals. As the need for more precise and accurate estimates of the Fourier harmonic 1/2 amplitudes increases, so does the cost of the experiment, both in researcher's time and facility

time. The important issue is that the random and systematic errors associated with distortion measurements should not be ignored, but handled within the proper statistical framework.

INTRODUCTION

The current development strategy for combat air-vehicles is directed towards reduction in the Life-Cycle Cost (LCC) with little or no compromise to air-vehicle performance and survivability. This strategy has been extended to the aircraft component level, in particular, the engine inlet diffuser system. One method to reduce inlet system LCC is to reduce its structural weight and volume. Consequently, advanced combat inlet configurations are being made more compact (or shorter) to achieve weight and volume (and LCC) reduction. However, compact S-duct diffusers are characterized by high distortion and low pressure recovery produced by extreme wall curvature and strong secondary flow gradients. These characteristics are further aggravated by maneuver conditions. Since survivability rather than aerodynamic performance often drives the inlet design, it is expected that the flow quality entering the turbine engine would present an additional challenging environment for both fan/compressor surge margin and aeromechanical vibration. Interest in High Cycle Fatigue (HCF) research by the US aerospace community has been spurred by discrepancies between the expected durability of engine components compared to that actually experienced in the field. Recognizing that inlet distortion is a forcing function for vibration in the fan components, methods for increasing HCF Life Expectancy can been combined with techniques for inlet recovery and engine face distortion management. Therefore, to enable acceptable performance levels in such advanced, compact inlet diffuser configurations, micro-scale secondary flow control (MSFC) methods are being developed to manage the recovery, distortion, and HCF aspects of these complex flow fields.[(1)-(2)]

A primary factor for inducing blade vibration in the engine is the coupling of an aerodynamic forcing function with the natural mode of elastic deformation of the blade.[(3)] The severity of the blade vibration depends upon the effectiveness of the energy input, which is determined by the forcing function along the blade and the blade mode shape. Circumferential total pressure distortion is usually considered a primary forcing function that has been associated with blade vibration. This circumferential total pressure distortion can be broken into elemental wave patterns and related to the cyclic blade loading in the rotational reference frame. It is the measurement of these elemental wave patterns of circumferential total pressure distortion during Wind Tunnel tests using standard rakes that has caused much uncertainty.

To understand more clearly the nature of excitation of the blade flexure modes, a Fourier (harmonic) analysis is usually performed on the steady state distortion pattern along a constant radius ring.[(4)] The circumferential distortion is thus broken up into discrete amplitudes at a “# per rev” frequency, and compared to the engine blade resonance frequencies. The frequency number in the harmonic analysis corresponds to the number of excitations per revolution. This discrete approximation incurs the Nyquist criteria for data sampling, i.e. the number of data points of sampling should be 2.0 times (sometime 2.5 times) the highest frequency of interest. This means that for a 40-probe rake with 8-arms, the cut off frequency is 4 per rev and the harmonic content can only be determined up to 3 per rev. The problem is to determine the appropraited sampling interval. Sampling too close yields correlated and highly redundant data, thus unnecessarily increasing the cost and labor of calculations. On the other hand, sampling points too far apart tends to confuse the high and low frequency portions of the data. The dilemma can be better understood if it is realized that the preciseness and accuracy of estimated Fourier coefficients depends both on

the number of data samplings and the complexity of the circumferential distortion pattern under analysis. In other words, the ability to measure (estimate) the Fourier harmonic components of a circumferential pattern within a Wind Tunnel environment using standard rakes depends both on the rake array used and the complexity of the distortion patterns being evaluated. However, the circumferential distortion patterns are not generally known *a priori*, and therefore the measuring rake cannot be optimally chosen to accurately measure (estimate) the Fourier harmonic amplitudes at the "# per rev" frequencies of interest. An alternate approach is to employ rotating rake methodologies. While these provide the necessary precision and accuracy of measurements, they require costly and lengthy 'stays' at each flow conditions within a Wind Tunnel experiment.

This "Catch 22" situation is however, not insurmountable. By combining the concepts of Computational Fluid Dynamics (CFD) analysis and Design of Experiments (DOE) methodologies,[5] a varied and significant set of cases can be economically defined and analyzed which represent a large range of distortion patterns of interest for a particular application. From this information, a optimal rake geometry array for Wind Tunnel tests can reasonably be defined that can precisely and accurately measure the amplitudes at the "# per rev" frequencies of importance. This overall combined methodology of using both CFD analysis and DOE methodologies to optimal choose a measurement rake array is the subject of this report. The objectives of this investigation is to quantify the effects of both (a) number of arms on the survey rake (with five probes per arm), and (b) degree of rake clocking on both the precision and accuracy of the distortion measurements and the resulting estimates of the Fourier harmonic 1/2 amplitudes of distortion, over a wide range of operating conditions.

NOMENCLATURE

AIP	Aerodynamic Interface Plane
c	Micro-Vane Effector Chord Length
CCF	Central Composite Face-Centered
CFD	Computational Fluid Dynamics
D	Engine Face Diameter
DOE	Design of Experiments
h	Micro-Vane Effector Blade Height
HCF	High Cycle Fatigue
Fi/2	i^{th} Fourier Harmonic 1/2 Amplitude
FM/2	Mean Fourier Harmonic 1/2 Amplitude
FRi/2	i^{th} Rake Fourier Harmonic 1/2 Amplitude
L	Inlet Diffuser Length
LCC	Life Cycle Costs
MSFC	Micro-Scale Secondary Flow Control
Mt	Inlet Throat Mach Number
n	Number of Micro-Vane Effectors per Band
PFAVE	Inlet Total Pressure Recovery
R	Inlet Throat Radius
Re	Reynold Number per ft.
RSM	Response Surface Methodology
$S_{y.x}$	Root Mean Square Error
X	Axial Distance

X_i	Generalize Regressor Variable
Y_i	Generalize Response Variable
α	Inlet Angle-of-Incidence
β	Micro-Vane Effector Angle-of-Incidence
γ	Inlet Angle-of-Yaw

RESULTS AND DISCUSSION

Design of the Experiment

The inlet flowpath chosen for this study featured a compact (L/D = 3.0), two turn, or S-duct inlet diffuser, Figure (1). This S-duct was defined by AGARD FDP Working Group 13 Test Case 3, Willmer, Brown and Goldsmith,[6] and was dubbed the DERA/M2129 inlet. Traditionally, this type of compact inlet duct would be excluded from design consideration since it is characterized by severe wall curvature that induces strong secondary flows. See Figure (1). This type of 3D flow separation, often called vortex liftoff, causes total pressure losses and severe engine face distortion. Figure (2) presents the engine face total pressure recovery contours and secondary flow velocity vectors for the DERA/M2129 inlet S-duct at a throat Mach number of 0.70. A vortex pair is dominant in the engine face flow field and this was accompanied by very severe engine face total pressure distortion.

To manage the flow in the DERA/M2129 inlet S-duct, a three-band installation arrangement of micro-scale effectors was placed in the upstream section near the inlet throat. See Figures (3) and (4). These micro-scale effectors were simple vanes, the largest height being about the average height of the momentum layer at the location of band (3), or about 2.0 mm. The purpose of these simple vanes was to create a set of co-rotating vortices that would quickly merge to form a thin layer of secondary flow that would counter the formation of the passage vortex pair.[1] Since the height of the vane effectors were limited to 2.0 mm, a multi-band arrangement was chosen to investigate the possibility of enhancing the effect of the individual band of vanes by adding more bands. The spacing between the bands is critical since interaction would occur between respective bands of effector units. The first band was placed at the inlet throat station, X/R = 0.0, while the second and third bands of micro-vane effectors were placed nominally at axial positions X/R = 1.0 and at X/R = 2.0 respectively. See Figure (3). Nominally, the spacing between the vane effectors was $\Delta X/c = 4.0$, i.e. about four effector chord length as measured between the half chord stations. See Figure (4).

In order to generate a wide range of operating conditions, a Design of Experiment (DOE) approach was used. The DOE chosen was a Central Composite Face-Centered (CCF) DOE in five fundamental operational variables, namely (1) vane heights in first effector band (h_1), (2) vane heights in second effector band (h_2), (3) vane heights in third effector band (h_3), (4) inlet angle-of-incidence (α), and (5) Reynolds number per ft. (Re). Table (1) shows the fundamental operational variables (factors) and the ranges studied. Table (2) shows the operational variables held constant throughout the study. Table (3) shows the responses for this study, which were the inlet total pressure recovery (PFAVE), and the first five Fourier harmonic 1/2 amplitudes (F1/2, F2/2, F3/2, F4/2, and F5/2) of engine face distortion. Table (4) shows the CCF Design-of-Experiment, and Figure (5) is the graphical representation of the CCF Design-of-Experiment used in this

study. Notice how the DOE efficiently spans a wide range of operating conditions in the five fundamental variables.

Each of the 27 cases in Table (4) were run with a Reynolds-averaged Navier-Stokes code[7] that allowed for numerical simulation of micro-vane effectors without the need to physically embed the vane effectors within the CFD grid structure. For the present study, however, the individual vanes were incorporated into the grid structure, and the appropriate boundary conditions applied to the individual vane effectors.The half-plane grid structure was composed of three blocks: an upstream block, a effector section containing the micro-vanes, and a downstream block. See Figures (3) and (4). The computational half-plane grid varied in total number of mesh points from about 750,00 to 1,500,000 depending on the micro-vane configuration. All CFD calculations were accomplished assuming half-plane symmetry. It was important to investigate the interactions between the separate effector bands without using the vane model in the code, so that proper band interaction could be established. This also established a set of baseline validation data to further verify the vane effector model in the Navier-Stokes code[7] for multi-band flow control design concepts. Figure (6) shows all the total pressure recovery contours corresponding the schedule of cases in Table (4). They cover a wide range of CFD solutions over an angle-of-incidences, Reynolds number conditions, and band installation geometries.

Harmonic Analysis of Distortion

The overall methodology used to obtain the Fourier harmonic content of inlet distortion was first proposed by Ludwig,[8], and is currently in use at the Williams International Corporation. This methodology is characterized by the use of radial weighting factors applied to the total pressure rake measurements to compress the rake information to a single radius ring of data samples. The weighting functions are shown in Table (5). The three measuring rakes used in this study (i.e, 40, 60, and 80 probes) each had 5 steady state probe positions located radially at the centers of equal areas on each of the rake arms. See Figure (6). Using the AIP instrumentation locations of Figure (6), the 27 CFD solutions were interpolated at each of the probe positions shown. The span-weighted average total pressure was calculated for each rake by multiplying the probe total pressure by the span-weighted coefficients, shown in Table (5), and adding the results over the five probes of the rakes to form a single radius ring of data samples. The number of data samples in each case corresponds to the number of arms in the respective survey rake. A Fourier analysis was then performed on the single radius ring of compressed span weighted average rake total pressures to determine the first five Fourier harmonic amplitudes (1/2 the peak-to-peak amplitudes) of engine face distortion.

A summary of the measurement techniques used in this study is presented in Table (7). It contains the three rake arrays shown in Figure (6), as well as a reference rake composed of 5 rings with 256 arms. The measurement techniques considered in this study included three rakes of 40-probes, 60-probes, and 80-probes, where each rake was both considered fixed in the 0° clocking angle, and “clocked” over 10 angles from 0° to the respective rake half-angle. Since there is half-plane symmetry in the distortions patterns, the rake half-angle was used in this data reduction. For a general distortion pattern, however, the full rake angle must be used in the data reduction.

One bit of explanation is warranted regarding the concept of “clocking” in this report. Clocking is not used to change the sampling interval, but rather to increase the accuracy of

the measurement at the sampling interval given by the number of arms in the survey rake. This is accomplished by taking the mean of 10 clocking angles over the given rake sampling interval. Thus the measurement with and without clocking each have the same sampling interval for a given survey rake, however the clocked rake will be shown to be more precise and accurate. A simply study was made on the 40-probe standard measurement rake to determine the appropriate number of clocking angles per sampling interval. Intervals of 5, 10 and 20 clocking angles per sampling interval were chosen. The results indicated that the mean results changed from 5 to 10 clocking angles, but remained essentially the same between 10 and 20 clocking angles.

Statistical Analysis of Rake Data

In order to understand the various kinds of random (precision) and systematic (biasing) errors that were introduced into the estimation of the Fourier harmonic 1/2 amplitudes as a result of the rake geometry and its use (i.e. whether "clocked" or not), an ordinary least square regression (OLR) was employed for analyzing the relationship between the compressed rake data and the reference or "true" value. Comparison of the Least Squares Regression line with the ideal functional relationship (i.e. one-to-one line of perfect agreement) provided important information as to the nature of error, either random (precision) or systematic (bias). The method of least squares defines the "best fitting" model to be the one that comes closet to the sample data in the sense of minimizing the sum of squared discrepancies between the observed response value Y_i and the respective value predicted by the regression model $\hat{Y}_i$. A simple linear regression model is given by the expression:

$$\hat{Y}_i = \beta_0 + \beta_1 X_i \qquad (1)$$

The slope β_1 and intercept β_0 of equation (1) are estimated by:

$$\hat{\beta}_1 = \frac{\sum_{i=1}^{N} (X_i - \bar{X})(Y_i - \bar{Y})}{\sum_{i=1}^{N} (X_i - \bar{X})^2} \qquad (2)$$

and

$$\hat{\beta}_0 = \bar{Y} - \hat{\beta}_1 \bar{X} \qquad (3)$$

where $\bar{X}$ is the mean of the independent or regressor variable:

$$\bar{X} = \frac{1}{N} \sum_{i=1}^{N} X_i \qquad (4)$$

and $\bar{Y}$ is the mean of the dependent or response variable:

$$\bar{Y} = \frac{1}{N} \sum_{i=1}^{N} Y_i \qquad (5)$$

and N is the total number of (X_i,Y_i) pairs in the data sample. The RMS error $S_{y.x}$ of the regression is given by:

$$S_{y \cdot x} = \sqrt{\frac{\sum_{i=1}^{N} (Y_i - \hat{Y}_i)^2}{(N-2)}} \qquad (6)$$

With 95.0% confidence, the actual or true line falls in the region bounded by the hyperbolic curves described by:

$$\pm 0.95 Y_i = \hat{Y}_i \pm t(0.975, N-2) S_{y \cdot x} \sqrt{\frac{1}{N} + \frac{(X - \bar{X})^2}{\sum_{i=1}^{N} (X_i - \bar{X})^2}} \qquad (7)$$

where $t(0.975, N-2)$ is the critical value from the t-table, $\bar{X}$ is the mean of the independent variable given by equation (4), and $\hat{Y}_i$ is the predicted response value using the regression model given by equation (1). Likewise, 95.0% confidence intervals can be placed on both the slope of the regression model, $\pm 0.95\beta_1$ and intercept of the regression model, $\pm 0.95\beta_0$ from the expressions:

$$\pm 0.95\beta_1 = \hat{\beta}_1 \pm t(0.975, N-2) \frac{S_{y \cdot x}}{\sqrt{S_x^{\,2}(N-1)}} \qquad (8)$$

$$\pm 0.95\beta_0 = \hat{\beta}_0 \pm t(0.975, N-2) S_{y \cdot x} \sqrt{\frac{1}{N} + \frac{\bar{X}^2}{S_x^2 (N-1)}} \qquad (9)$$

where S_x^2 is given by the expression:

$$S_x^2 = \frac{\sum_{i=1}^{N} (X_i - \bar{X})^2}{(N-1)} \qquad (10)$$

For the analysis in this paper, Y_i is the measured metric value from the survey rake and X_i is the reference or true metric value from the reference rake.

Effect of Rake Array and Clocking

The performances of three rakes, (i.e. the 40-probe, 60-probe and the 80-probe rake arrays) both at the fixed 0° clocking position and over the 10 clocking angles are presented in Figures (8) through (13). Each figure contains six graphs. The first graph presents the engine face

area average total pressure determined from the computational grid (PFAVE) compared either to that measured by the rake (PR) in the fixed 0° clocking position or the mean of 10 rake clocking angles (PM). The additional five graphs in each figure shows a comparisons between the reference Fourier harmonic 1/2 amplitude (Fi/2, i=1,5), i.e. the Fourier harmonic amplitude determined from the reference 256 arm rake array, and either the Fourier harmonic 1/2 amplitude from the single fixed 0° rake position (FRi/2, i=1,5) or the mean Fourier harmonic 1/2 amplitude (FMi/2, i=1,5) determined from the 10 clocking angles. Presented in each figure is the one-to-one line of perfect agreement (ideal relationship) between the reference metric and the measured metric. Accompanying each graph is the least square regression of the respective reduced rake data, determined from equations (1) through (5), and the 95% confidence interval on the true regression line given by equation (8).

The various kinds of biasing errors that occurred for the 40-probe rake at to 0° clocking angle can be seen by comparing the least square regression line with the ideal functional relationship in Figure (8). If the one-to-one line of perfect agreement (ideal line) falls completely within the 95% confidence interval on the true line, then there is no bias (i.e. regression line is not statistically significantly different from the line of perfect agreement). To augment these visual summaries, the results of the calculating the 95% confidence intervals on the slopes and intercepts are presented in Tables (8) through (13) for the six scenarios (i.e. 40, 60, and 80 probe rake arrays with and without clocking). These are also useful in assessing measurement biasing. If the 95% confidence interval on the slope contains the number one and the 95% confidence interval on the intercept contains the number zero, then the regression line is not statistically different from the ideal or one-to-one line of perfect agreement. However, confidence intervals on the intercept that are far removed from the origin (i.e. (X,Y) = 0.0) can be unusually large and therefore meaningless. Hence testing the intercept for PFAVE in this study was not applicable (i.e. N/A). Testing for bias by testing on the slope of PFAVE for being significantly different from one and testing whether the one-to-one line of perfect agreement falls within the 95% confidence interval of the true regression line are both valid and meaningful.

For example, in Figure (8) the one-to-one line of perfect agreement does not fall within the confidence interval on the true line for the first Fourier harmonic 1/2 amplitude. Hence, the FR1/2 is biased or statistically different from the ideal measurement. The graph in Figure (8) also shows the nature of the bias. It appears that the slope is not different from the one-to-one line (i.e. they are parallel), but there is a constant positive bias. This is shown to be the case in Table (8) where the 95% confidence interval on the slope contains the number one, but the 95% confidence interval on the intercept does not contain the number zero. The entire interval is positive, hence the notation of constant positive bias. Notice, that these findings are easier to see visually in the figures that show the 95% confidence interval on the true line, but are substantiated in the tables that provide the 95% confidence on the slopes and intercepts. In Figure (8), it is of particular interest to see the nature of the bias for the fourth and fifth Fourier harmonic 1/2 amplitudes of engine face distortion. Note that the bias is not a simple constant offset as was the case for the first, second, and third Fourier harmonic 1/2 amplitudes. The bottom line is that the non-clocked 40-probe rake leads to serious biasing (systematic) errors as well as large random (precision) errors.

In Figure (9) and Table (9) the dramatic effect of simply clocking the 40-probe rake can be seen. There is no bias in PFAVE nor in the second Fourier harmonic 1/2 amplitudes of distortion. While slight biases are detectable in the first, third and fourth Fourier harmonic 1/2

amplitudes, there is a substantial bias in the fifth Fourier harmonic 1/2 amplitude. Figure (10) and Table (10) show the results for the 60-probe rake array at the single 0° clocking angle. Biases are much better than with the 40-probe rake without clocking, but still evident. Figure (11) and Table (11) show the dramatic effect of clocking the 60-probe rake. Most evidence of bias has vanished. Figure (12) and Table (12) show the results for the 80-probe rake at the single 0° clocking angle. As was the case in going from 40-probe to 60-probes, adding 20 more probes greatly reduced the bias. Only slight detectable biases exist. Lastly, Figure (13) and Table (13) show the results of clocking the 80-probe rake.

The Nyquist criteria is a number determined through a specific mathematical analysis that indicates the absolute minimum number of samples required to resolve a discrete frequency out of a complex wake form. Figure (8) and (9) presents the measurement results for a 40-probe rake at the same sampling interval without and with clocking. The Nyquist means that with 8 arms (circumferential positions) the cutoff frequency for the 40-probe rake is 4 per rev. and the harmonic content can only be determined up to 3 per rev. The validity of the Nyquist can clearly be seen in Figure (9), were clocking was used to decrease the random and systematic errors of the 40-probe rake results. However, it is not obvious in Figure (8) that the Nyquist criteria is valid for the single 0° clocking angle results since large precision and biasing errors mask the measurement results. The Nyquist criteria for the 60-probe rake states that the cutoff frequency is 6 per rev. and the harmonic content can only be determined up to 5 per rev. The results for the 60-probe rake are presented in Figures (10) and (11), and it is evident that the more precise and accurate clocked results, Figure (11), satisfy the Nyquist criteria, while it is not obvious that the Nyquist criteria is valid for the single 0° clocking angle results in Figure (10), where large precision and biasing errors hide the results.

Table (14) contains the random RMS error ($S_{y.x}$) about each regression line scenario. Note that clocking the rake greatly reduced $S_{y.x}$ random (scatter about the regression line) error. The random error also, in general, decreased with increasing the number of arms (i.e. number of total probes) on the engine face survey rake. Occasionally, large variations in the survey rake results occurred. This resulted in part because of the occurrences of anomalies. Because there was a relatively small number of measuring location on the engine face rakes (between 40 and 80 probes in this study), the rake occasionally “caught” an abnormally large number of either low or high total pressure values. These anomalies also produced very large variations in the Fourier harmonic analysis of the distortion pattern. Averaging the clocked metric values results in better agreement with the reference or true metric values. A single 0° clocking angle data point would therefore leave open the possibility of gross measurement error, which could not be identified or labeled. Ultimately, this shows up as a larger random measurement error component for the case of the 0° clocking angle data sample.

One bit of explanation is warranted regarding these confidence intervals. The amount of scatter in the data also affects the results. The “nosier” the data (i.e. the larger the standard deviation of the regression, ($S_{y.x}$) the larger the confidence interval becomes. Larger confidence intervals tend to lead to the conclusion that there is no bias. While this may be statistically true, it is a poor trade-off for having larger random measurement errors. There may be no detectable bias, but the random measurement variation is poor. The opposite is also true. If there is very little scatter in the data (i.e. about the fitted regression line), the $S_{y.x}$ is very small and the 95% confidence intervals become extremely tight leading to the conclusion of a significant, detectable

bias (i.e. see for example the fourth Fourier harmonic 1/2 amplitude for the 80-probe rake). So one must view the data and statistical results with a properly focused eye, taking into account the amount of random error in the data, and thus the standard warning of statistical versus practical differences.

Even with the caveats described in the previous paragraph, the differences between the 40, 60, and 80-probe rake arrays with and without clocking were dramatic. Hence, both random (precision) and systematic (biasing) measurement error improved with clocking the engine face rake.

CONCLUSIONS

By combining the concepts of CFD analysis and Design of Experiments methodologies, a varied and significant set of cases can be defined and analyzed which can represent a large range of distortion patterns for a particular application. From the information gathered from this methodology, a rake geometry for use in Wind Tunnel tests can reasonably be defined which precisely and accurately measures the amplitudes at the "# per rev" frequencies of interest. Three rake arrays were considered for this study, a 40-probe, 60-probe and 80-probe array, while two methods of acquiring the data from each of these rake arrays were examined. One method of acquiring probe data was to fix each of the rake arrays in its 0° clocking angle and acquire a single set of probe data. The second approach was to clock each of the rake arrays over ten locations between the 0° clocking angle and the respective rake angle. In general, as the number of arms on the rake array increased, both random and systematic errors associated with measurement of the Fourier harmonic 1/2 amplitudes decreased. Clocking the rake and using the mean of ten clocking angles to represent the metric of interest also improved both precision and accuracy. The 40-probe rake array, recommended by the SAE S-16 committee,[9] probably provided random and systematic measurement errors that were too large to be of value. The 60-probe rake array used with clocking gave both very low random and systematic measurement errors up through the fourth Fourier harmonic 1/2 amplitude.The 80-probe rake with clocking provided both low random and systematic measurement errors up through the fifth Fourier harmonic 1/2 amplitude. In deciding the performance of different rake arrays to precisely and accurately provide estimates of the Fourier harmonic 1/2 amplitudes, consideration must be give as to whether clocking would be used in the data acquisition. Large reductions in both random and systematic measurement errors can be realized by clocking the engine face rake.

In general, the kind of survey rake that is chosen for a Wind Tunnel experiment and the rake methodology used in providing the total pressure data needed to estimate the Fourier harmonic 1/2 amplitudes depends on the researcher objectives and what magnitude of both random and systematic errors are acceptable within the stated goals. The more precise and accurate the estimate of Fourier harmonic 1/2 amplitudes that are needed, the more expensive the experiment, both in researcher's time and facility time. The important issue is that the errors associated with distortion measurements should not be ignored, but handled within the proper statistical framework.

REFERENCES

(1) Anderson, B. H., Miller, D. M., Yagle, P. J, and Truax, P. P., "A Study of MEMS Flow Control for the Management of Engine Face Distortion in Compact Inlet Systems," FEDSM99-6920, 3rd ASME/JSME Joint Fluids Engineering Conference, San Francisco, CA, July 18-23, 1999.

(2) Hamstra, J. W., Miller, D. N., Truax, P. P., Anderson, B. H., and Wendt, B. J., "Active Inlet Flow Control Technology Demonstration", ICAS-2000-6.11.2, 22nd International Congress of the Aeronautical Sciences, Harrogate, UK, August 27th-September 1st, 2000.

(3) Hamed, A., Numbers, K., "Inlet Distortion Considerations for High Cycle Fatigue in Gas Turbine Engines", AIAA 97-3364, 33rd AIAA/ASME/SAE/ASEE Joint Propulsion Conference & Exhibit, Seattle, WA, July 6th-9th, 1997.

(4) Cousins, William T., "Technique for the Development of Mechanical Limits", Pratt & Whitney Internal Correspondence, Jan. 2002.

(5) Box, E. P., Hunter, W. G., "Statistics for Experimenters", John Whiley & Sons, 1978.

(6) Goldsmith, E. L. and Seddon, J. (eds), "Practical Intake Aerodynamics," Blackwell Scientific Publications, Oxford, 1993.

(7) Bender, E. E, Anderson, B. H., and Yagle, P. J., "Vortex Generator Modeling for Navier Stokes Code", FEDSM99-69219, 3rd ASME/JSME Joint Fluids Engineering Conference, San Francisco, CA, July 18-23, 1999.

(8) Ludwig, G. R., "Aeroelastic Considerations in the Measurement of Inlet Distortion", 3rd National Turbine Engine High Cycle Fatigue Conference, 1998.

(9) SAE Aerospace Council Division Technical Committee S-16, "Gas Turbine Engine Inlet Flow Distortion Guidelines", ARP-1420, March 1978.

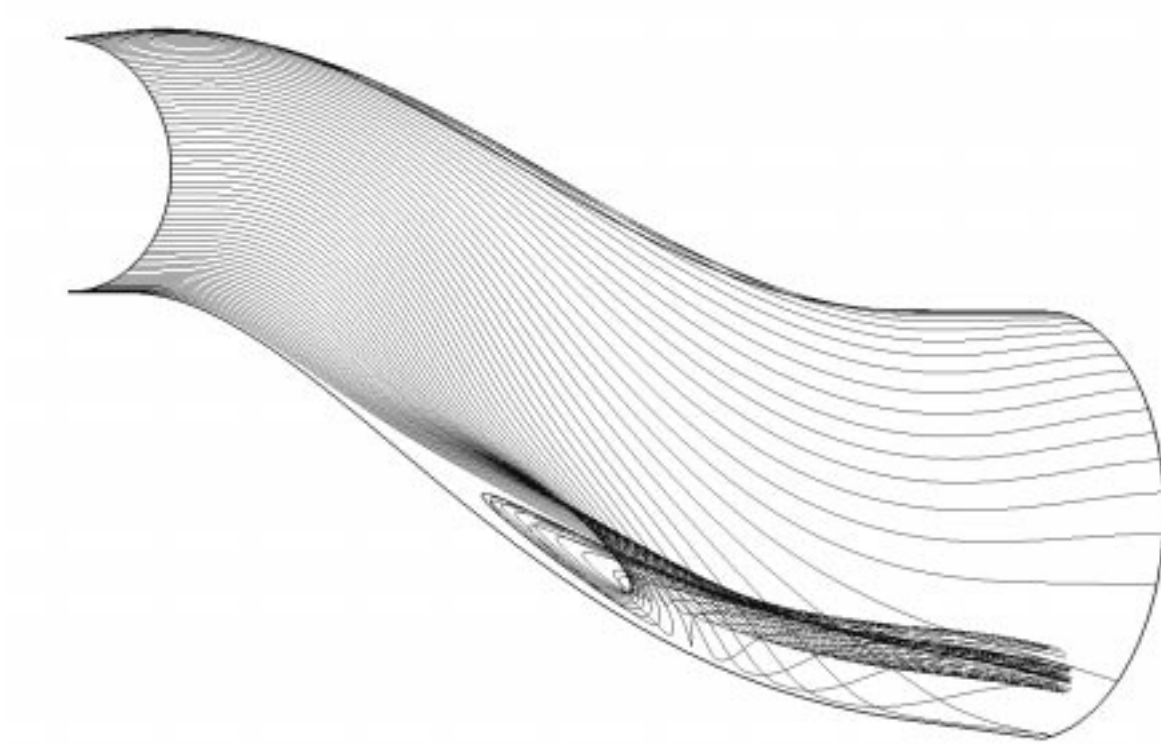

Figure (1): Particles traces showing the vortex liftoff (separation) within the DERA/M2129 inlet S-duct, Mt = 0.70, Re = 4.0 x 10^6 /ft., α = 0.0^o.

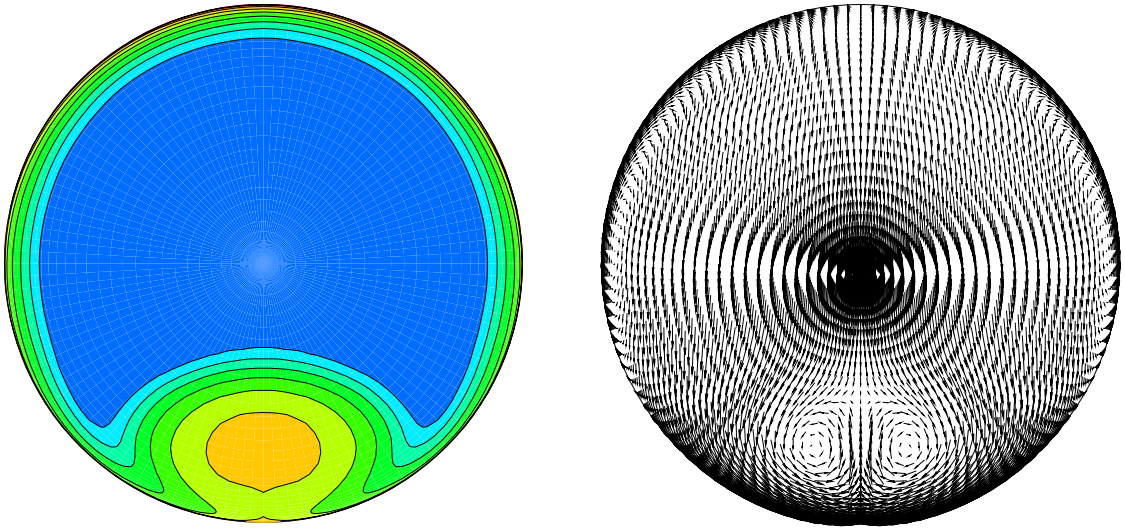

(a) Total Pressure Recovery Contours **(b) Secondary Flow Velocity Vectors**

Figure (2): Baseline engine face solution, Mt = 0.70, Re = 4.0 x 10^6 /ft., α = 0.0^o.

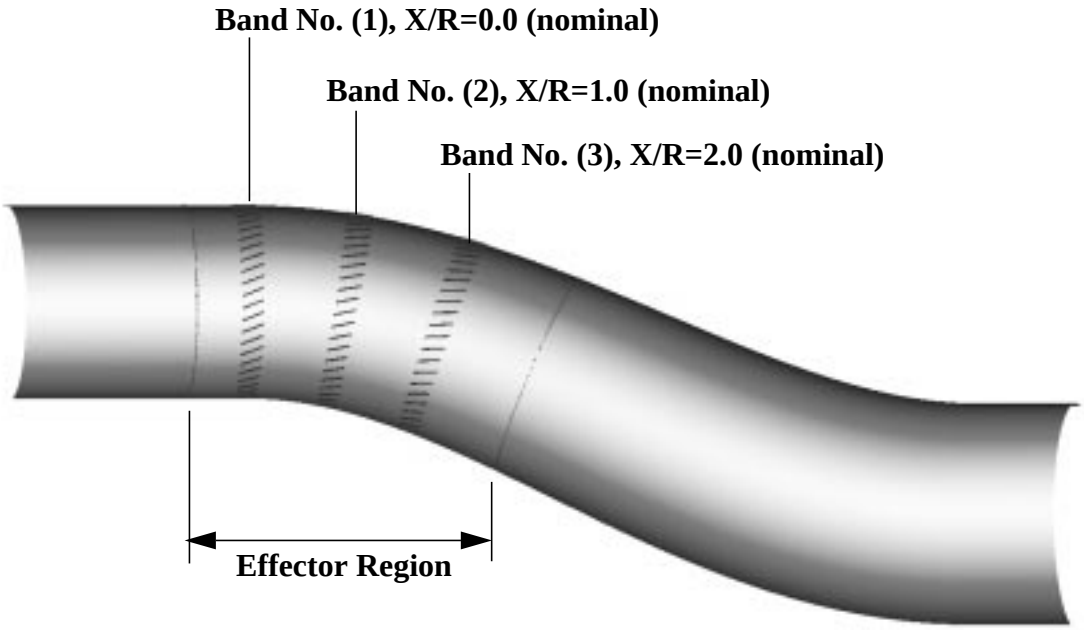

Figure (3): Location of effector region within the DERA/M2129 inlet S-duct.

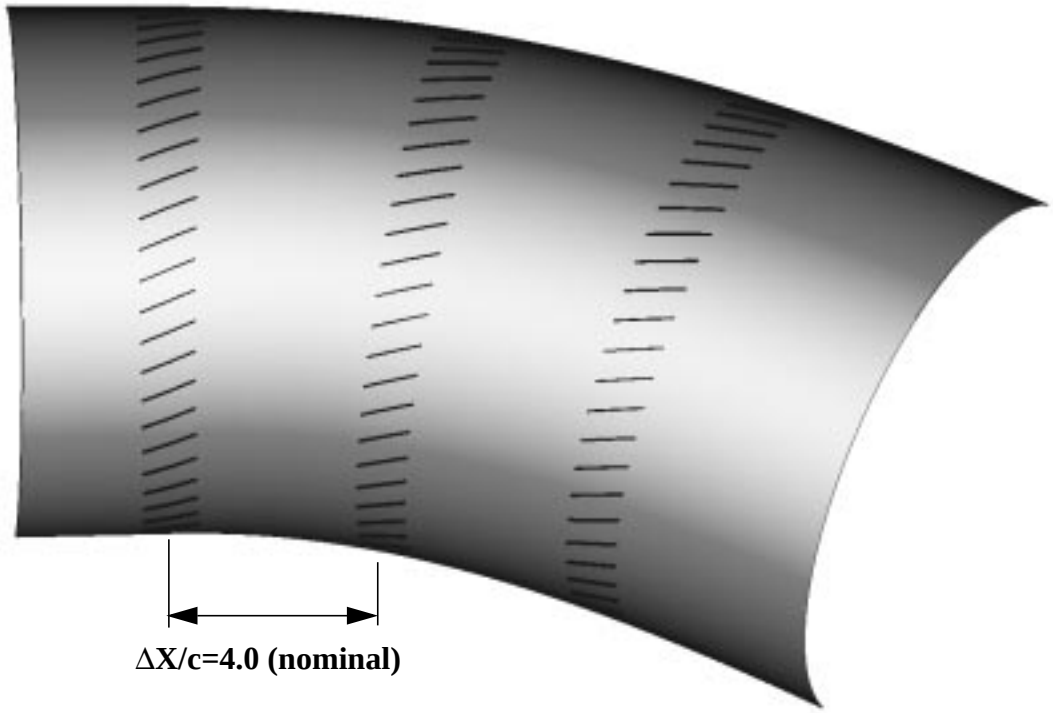

Figure (4): Micro-scale micro-vane arrangement within effector region.

Factors	Range
Installation Vane Height (mm), h_1	0.0 to 2.0
Installation Vane Height (mm), h_2	0.0 to 2.0
Installation Vane Height (mm), h_3	0.0 to 2.0
Inlet Angle-of-Incidence, (degs.), α	0.0^o to 20.0^o
Reynolds Number per ft. Re	$4.0x10^6$ to $20.0x10^6$

Table (1): Factors which establish the DOE design matrix.

Variable	Value
Number of Micro-Vane Effectors Units, $n_{i,\ i=1,3}$	24
Micro-Vane Angle-of-Incidence, (degs.), $\beta_{i,\ i=1,3}$	24.0^o
Micro-Vane Chord Length (mm), $c_{1,\ i=1,3}$	16.0
Throat Mach Number, Mt	0.700
Inlet Angle-of-Yaw, (degs.), γ	0.0^o

Table (2): Variables held constant

.

Design Responses	Nomenclature
Engine Face Total Pressure Recovery	PFAVE
1st Fourier Harmonic 1/2 Amplitude	F1/2
2nd Fourier Harmonic 1/2 Amplitude	F2/2
3rd Fourier Harmonic 1/2 Amplitude	F3/2
4th Fourier Harmonic 1/2 Amplitude	F4/2
5th Fourier Harmonic 1/2 Amplitude	F5/2

Table (3): DOE design responses

Config.	h_1	h_2	h_3	α	Re
nvg701	0.0	0.0	0.0	0.0	20.0
nvg702	2.0	0.0	0.0	0.0	4.00
nvg703	0.0	2.0	0.0	0.0	4.00
nvg704	2.0	2.0	0.0	0.0	20.0
nvg705	0.0	0.0	2.0	0.0	4.00
nvg706	2.0	0.0	2.0	0.0	20.0
nvg707	0.0	2.0	2.0	0.0	20.0
nvg708	2.0	2.0	2.0	0.0	4.00
nvg709	0.0	0.0	0.0	20.0	4.00
nvg710	2.0	0.0	0.0	20.0	20.0
nvg711	0.0	2.0	0.0	20.0	20.0
nvg712	2.0	2.0	0.0	20.0	4.00
nvg713	0.0	0.0	2.0	20.0	20.0
nvg714	2.0	0.0	2.0	20.0	4.00
nvg715	0.0	2.0	2.0	20.0	4.00
nvg716	2.0	2.0	2.0	20.0	20.0
nvg717	0.0	1.0	1.0	10.0	12.0
nvg718	2.0	1.0	1.0	10.0	12.0
nvg719	1.0	0.0	1.0	10.0	12.0
nvg720	1.0	2.0	1.0	10.0	12.0
nvg721	1.0	1.0	0.0	10.0	12.0
nvg722	1.0	1.0	2.0	10.0	12.0
nvg723	1.0	1.0	1.0	0.0	12.0
nvg724	1.0	1.0	1.0	20.0	12.0
nvg725	1.0	1.0	1.0	10.0	4.00
nvg726	1.0	1.0	1.0	10.0	20.0
nvg727	1.0	1.0	1.0	10.0	12.0

Table (4): Central Composite Face-Centered (CCF) DOE design.

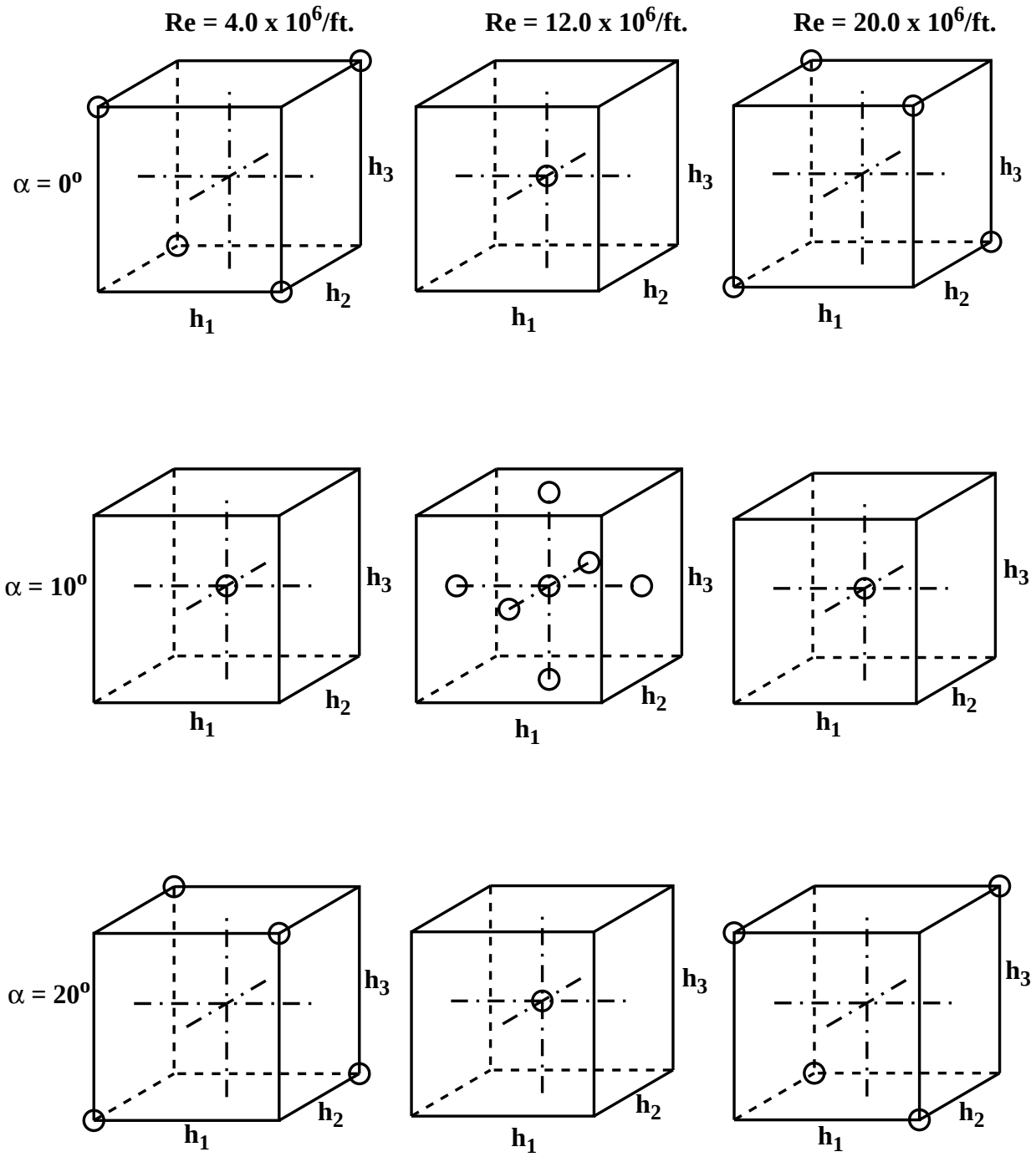

Figure (5): Graphical representation of the Central Composite Face-Centered (CCF) DOE design

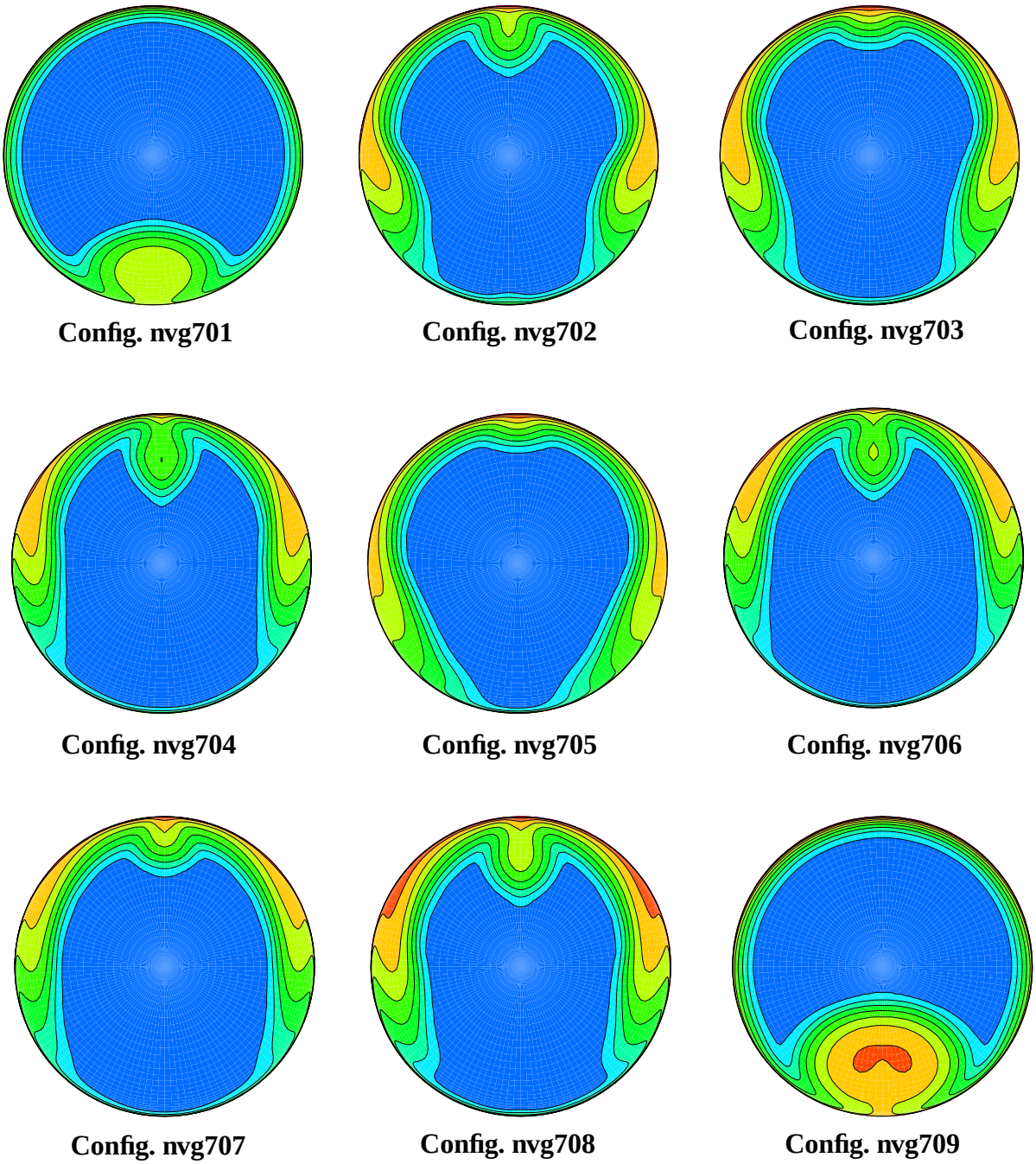

Figure (6): Total pressure recovery contours from the CFD analysis.

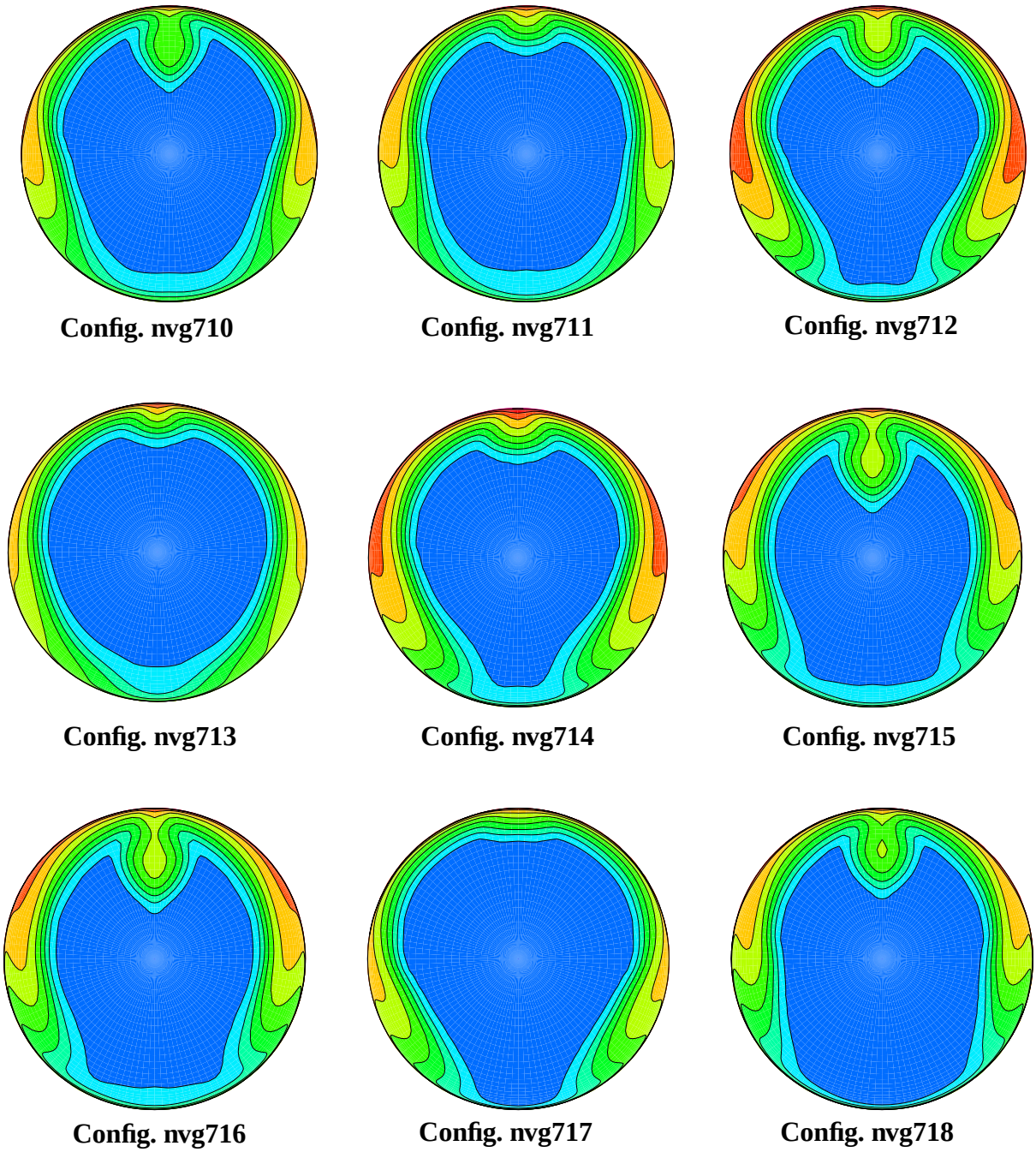

Figure (6): Total pressure recovery contours from the CFD analysis.

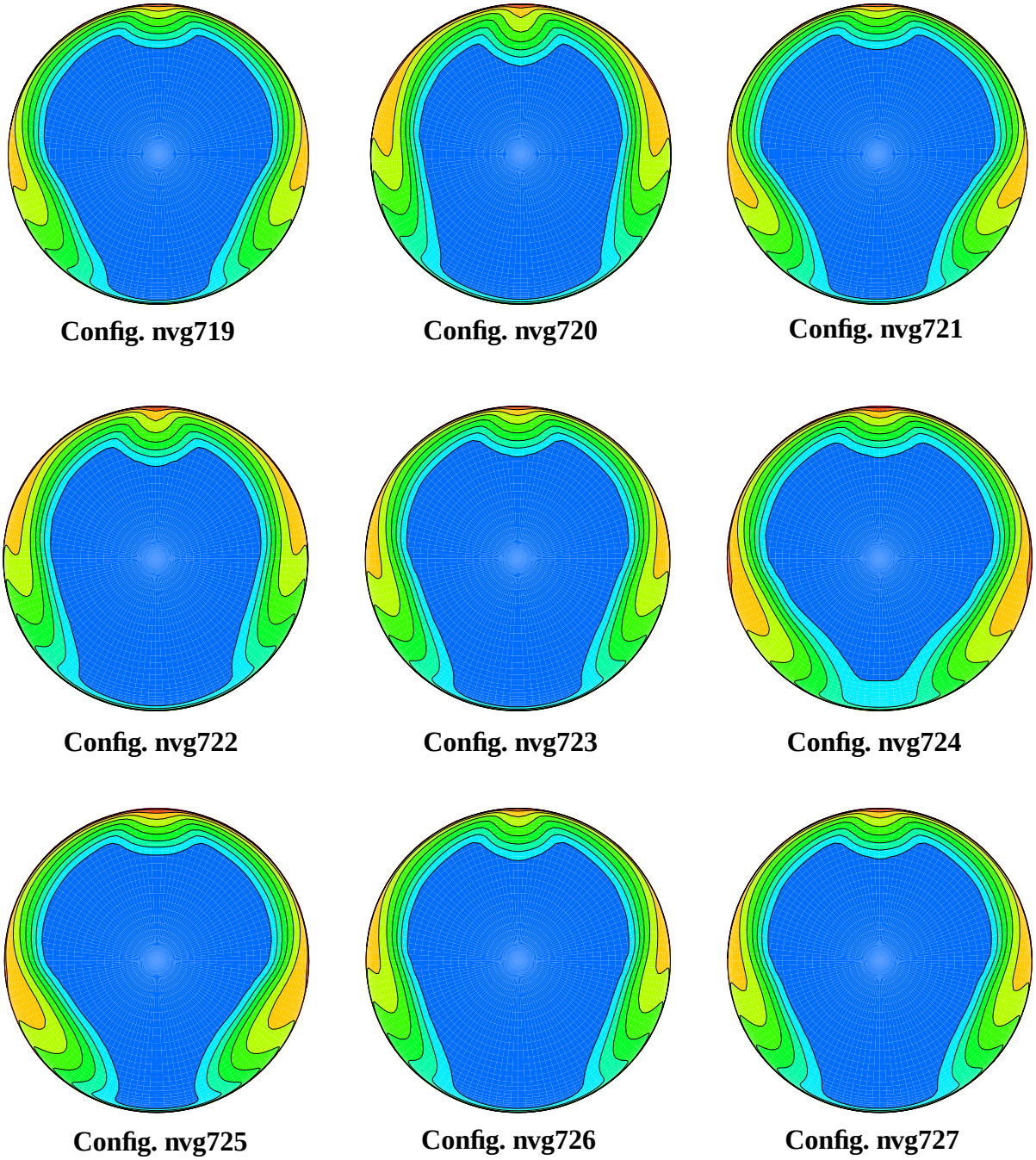

Figure (6): Total pressure recovery contours from the CFD analysis.

Ring Number	Radial Weighting Coefficient
1	0.05651
2	0.14248
3	0.21077
4	0.26918
5	0.32106

Table (6): Radial weighting coefficients applied to the total pressure rake measurements.

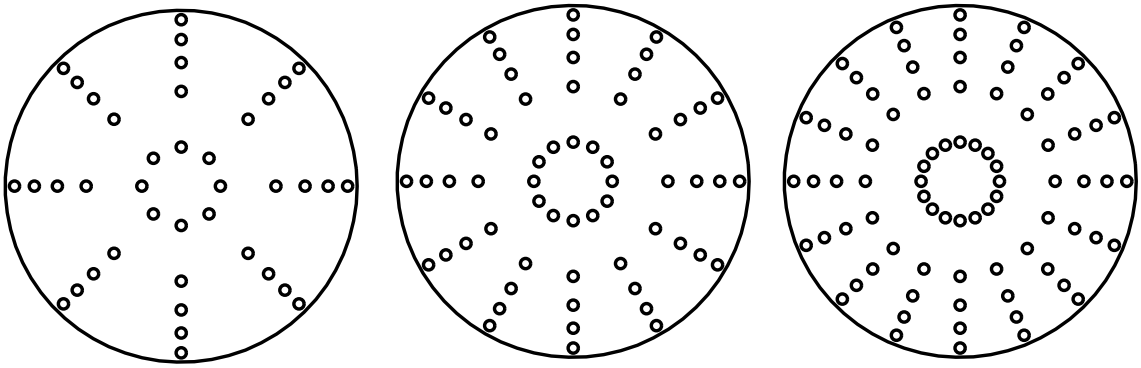

40-probe rake **60-probe rake** **80-probe rake**

Figure (7): Total pressure and distortion measurement arrays.

rake	No. of Rings	No. of Arms	Comments
40-probe	5	8	0° Clocking Angle
	5	8	10 Clocking Angles
60-probe	5	12	0° Clocking Angle
	5	12	10 Clocking Angles
80-probe	5	16	0° Clocking Angle
	5	16	10 Clocking Angles
Reference	5	256	0° Clocking Angle

Table (7): Definition of data acquisition techniques used in the study.

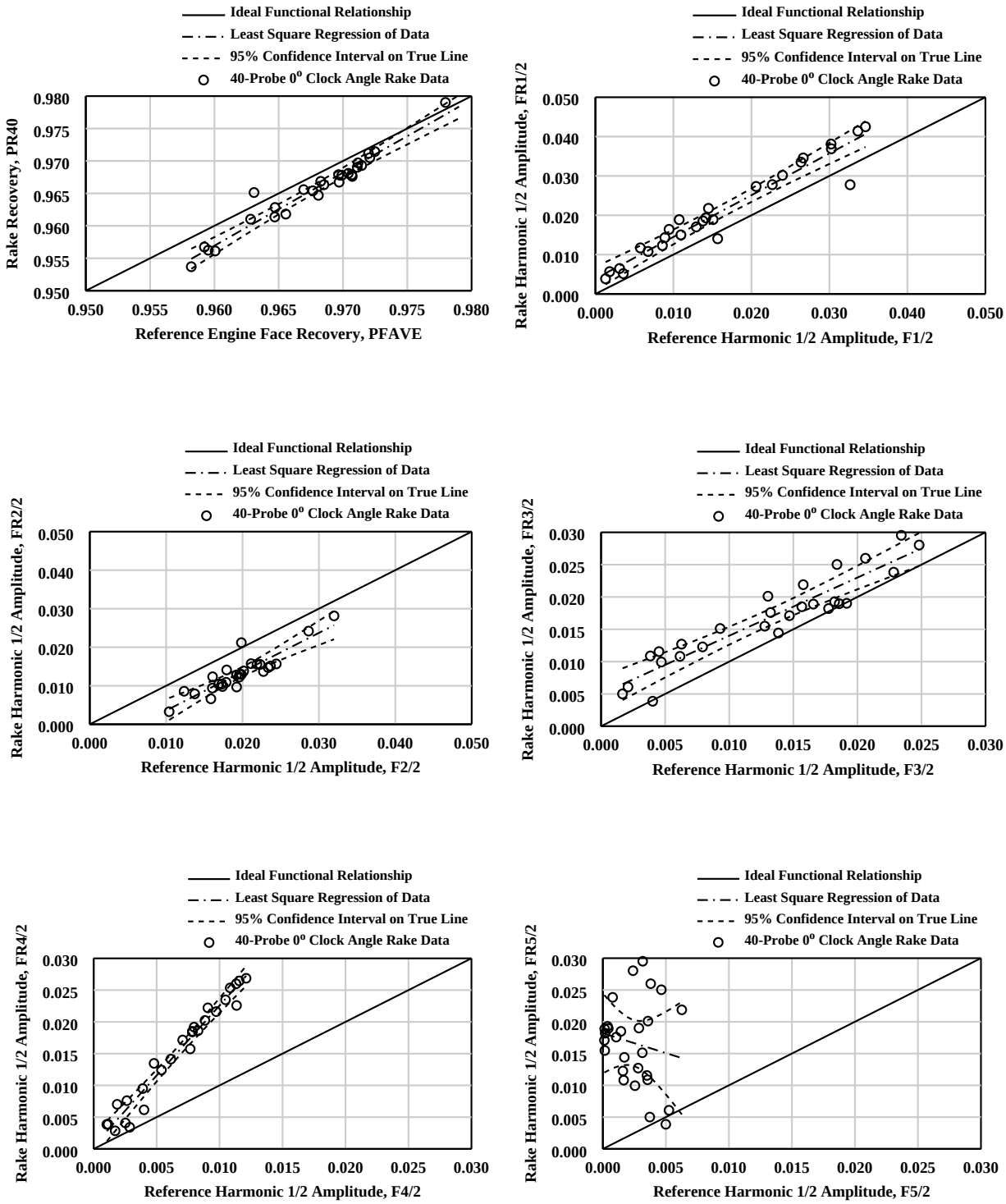

Figure (8): Measurement of engine face total pressure recovery and Fourier harmonic 1/2 amplitudes for the 40-probe rake positioned at the 0.0° clocking angle.

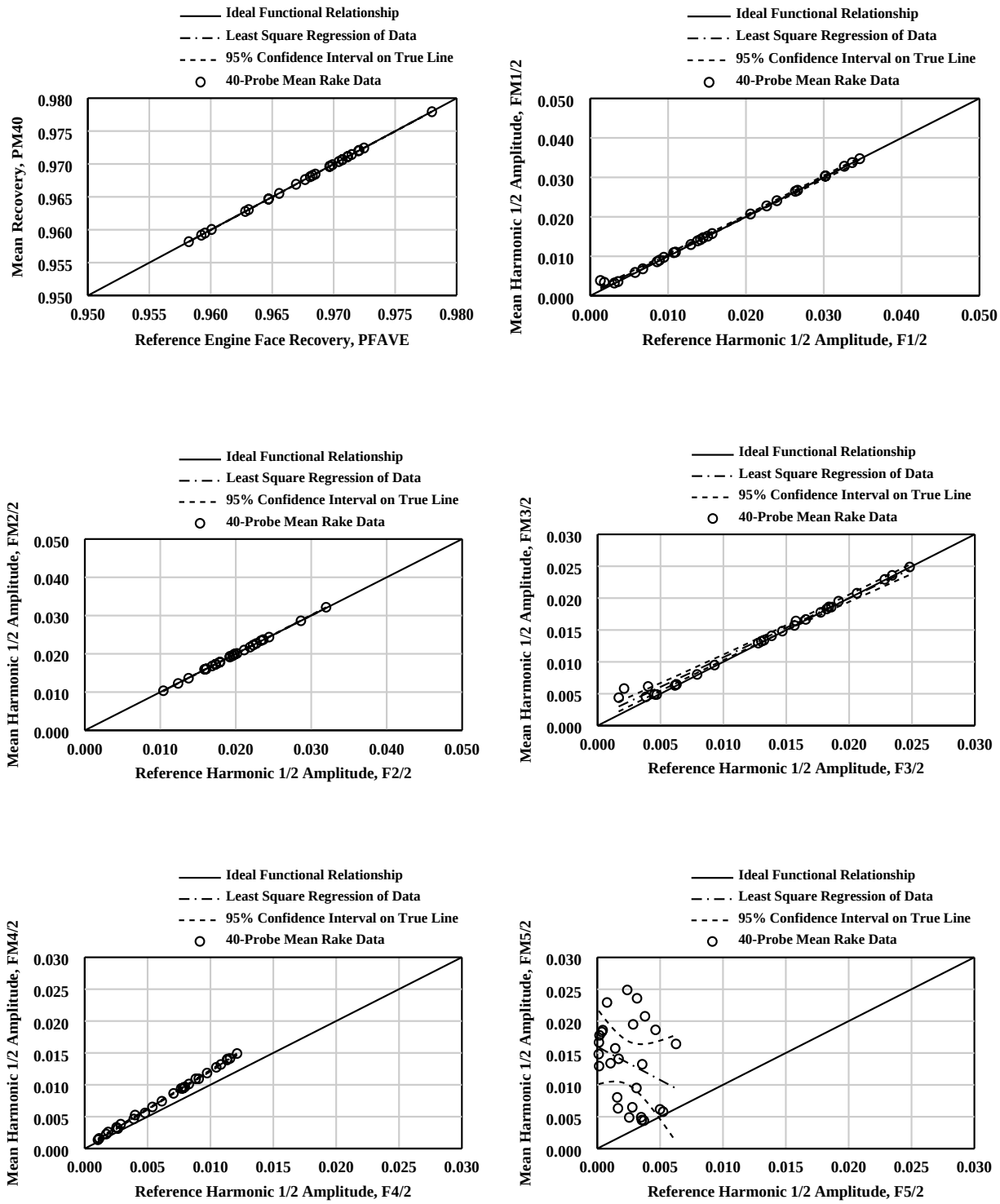

Figure (9): Measurement of engine face total pressure recovery and Fourier harmonic 1/2 amplitudes for the 40-probe rake, mean of 10 clocking angles.

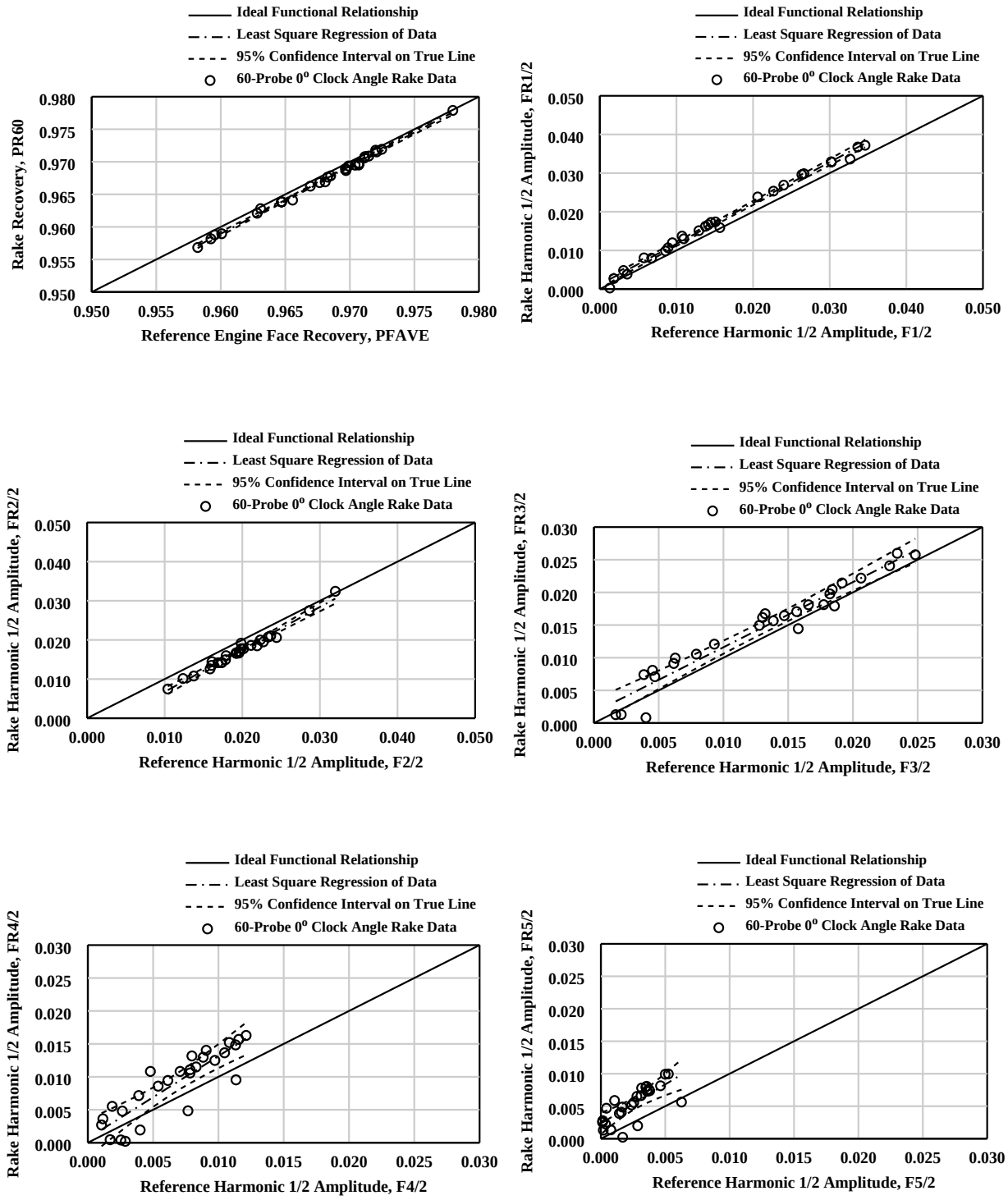

Figure (10): Measurement of engine face total pressure recovery and Fourier harmonic 1/2 amplitudes for the 60-probe rake positioned at the 0.0° clocking angle.

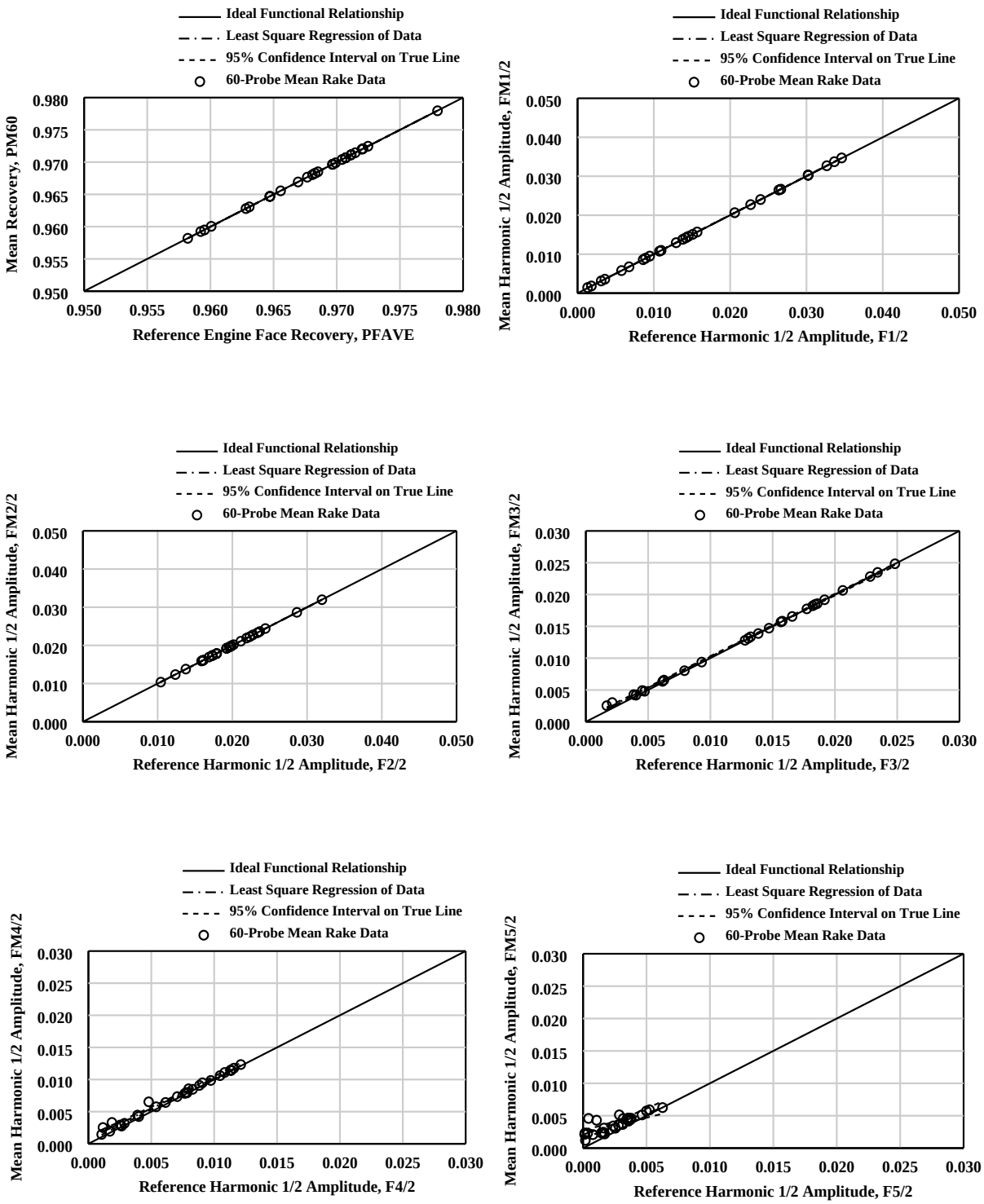

Figure (11): Measurement of engine face total pressure recovery and Fourier harmonic 1/2 amplitudes for the 60-probe rake, mean of 10 clocking angles.

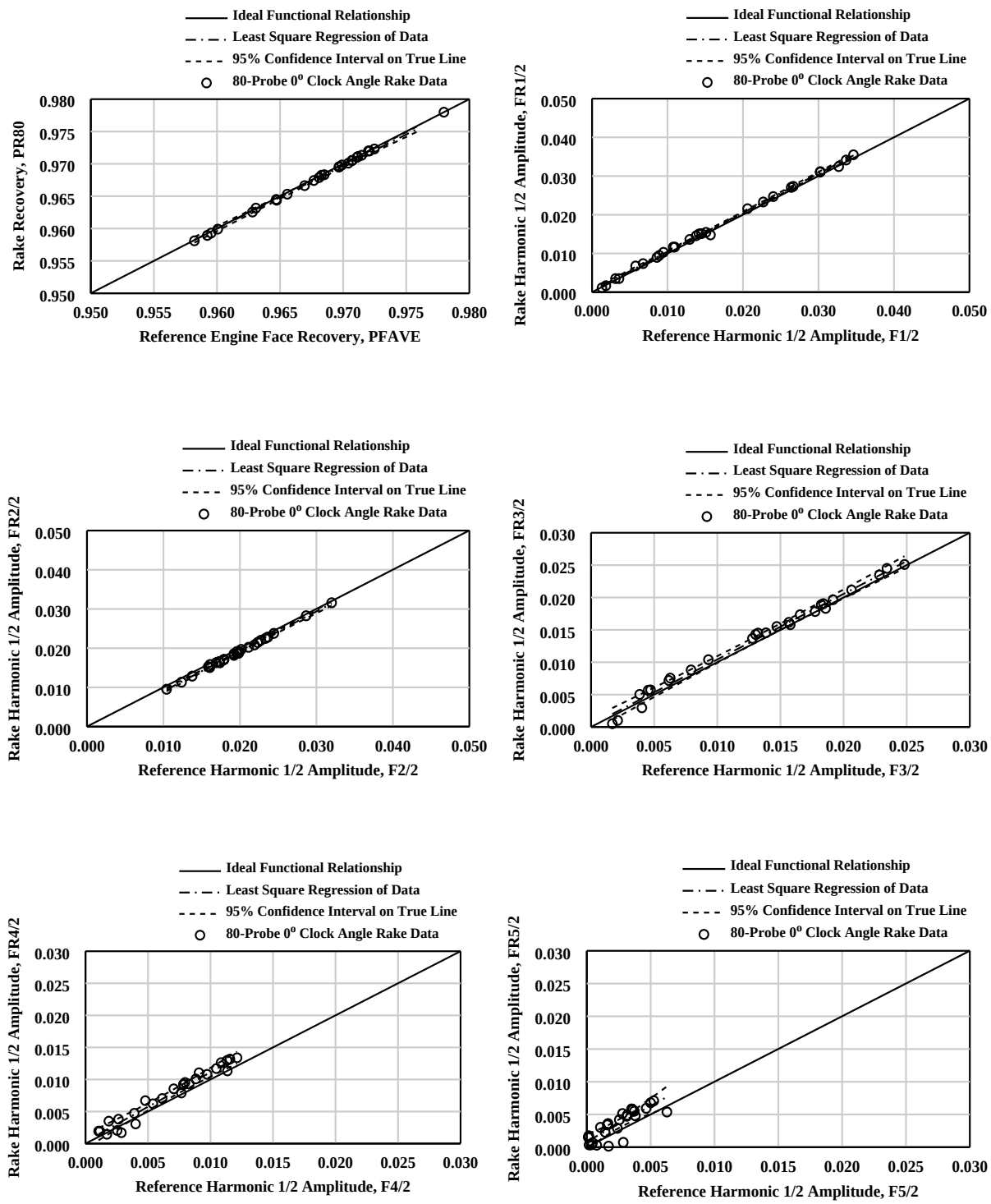

Figure (12): Measurement of engine face total pressure recovery and Fourier harmonic 1/2 amplitudes for the 80-probe rake positioned at the 0.0° clocking angle.

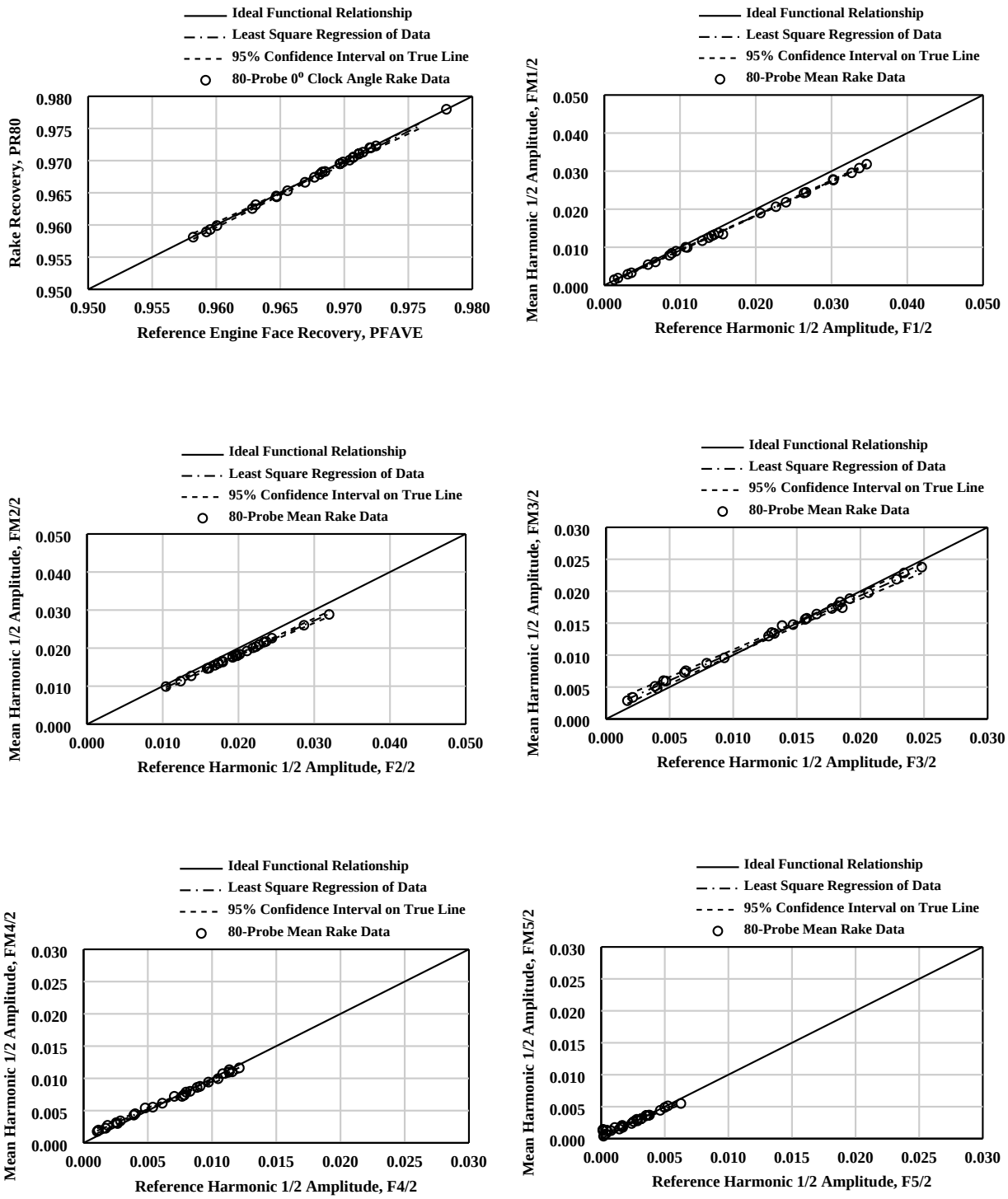

Figure (13): Measurement of engine face total pressure recovery and Fourier harmonic 1/2 amplitudes for the 80-probe rake, mean of 10 clocking angles.

Coeff.	PR40	F1/2	F2/2	F3/2	F4/2	F5/2
$-0.95\beta_0$	N/A	0.001340	-0.011934	0.002593	-0.001120	0.013038
β_0	0.124135	0.003876	-0.006487	0.005001	0.000484	0.018184
N/A	N/A	0.006412	-0.001042	0.007419	0.002089	0.023328
$-0.95\beta_1$	0.979701	0.905432	0.729268	0.713621	1.9169214	-2.732177
β_1	1.126118	1.061497	1.007001	0.899779	2.209955	-0.621464
$+0.95\beta_1$	1.272536	1.217562	1.284755	1.085937	2.450695	1.489248

Table (8): 95% confidence intervals on the regression intercept (β_o) and slope (β_1) for the 40-probe rake data at 0° clocking angle.

Coeff.	PR40	F1/2	F2/2	F3/2	F4/2	F5/2
$-0.95\beta_0$	N/A	0.000173	-0.000323	0.000681	-0.000011	0.011287
β_0	-0.000474	0.000604	-0.000143	0.001438	0.000145	0.015995
$+0.95\beta_0$	N/A	0.001342	0.000036	0.002195	0.000390	0.020861
$-0.95\beta_1$	0.999229	0.952495	0.997859	0.868780	1.183563	-3.038459
β_1	1.000469	0.978984	1.000701	0.927171	1.206991	-1.041684
$+0.95\beta_1$	1.001709	1.005473	1.016173	0.985562	1.230420	0.955092

Table (9): 95% confidence intervals on the regression intercept (β_o) and slope (β_1), 40-probe mean rake data from 10 clocking angles

Coeff.	PR60	F1/2	F2/2	F3/2	F4/2	F5/2
$-0.95\beta_0$	N/A	0.000384	-0.005976	-0.000107	-0.001864	0.000984
β_0	-0.036689	0.001557	-0.004087	0.001319	0.000654	0.002387
$+0.95\beta_0$	N/A	0.001927	-0.002198	0.003371	0.003173	0.003673
$-0.95\beta_1$	1.007327	1.008240	0.986845	0.863049	0.871069	0.652608
β_1	1.037126	1.055711	1.083186	0.997197	1.248951	1.204304
$+0.95\beta_1$	1.070525	1.103174	1.179527	1.131345	1.626833	1.756000

Table (10): 95% confidence intervals on the regression intercept (β_o) and slope (β_1) for the 60-probe rake data at 0° clocking angle.

Coeff.	PR60	F1/2	F2/2	F3/2	F4/2	F5/2
$-0.95\beta_0$	N/A	0.000012	-0.000057	0.000284	0.000385	0.001526
β_0	-0.000454	0.000034	0.000011	0.000463	0.000778	0.002085
$+0.95\beta_0$	N/A	0.000056	0.000079	0.000642	0.001172	0.002643
$-0.95\beta_1$	0.999407	0.999076	0.996097	0.961986	0.884653	0.435396
β_1	1.000461	1.000437	0.999589	0.975765	0.943677	0.664618
$+0.95\beta_1$	1.001515	1.001798	1.003082	0.989545	1.002701	0.893840

Table (11): 95% confidence intervals on the regression intercept (β_o) and slope (β_1), 60-probe mean rake data from 10 clocking angles.

Coeff.	PR80	F1/2	F2/2	F3/2	F4/2	F5/2
$-0.95\beta_0$	N/A	-0.000027	-0.001960	-0.000608	-0.000626	-0.000085
β_0	0.0286456	0.000352	-0.001148	0.000293	0.000332	0.000840
$+0.95\beta_0$	N/A	0.000732	-0.000339	0.000119	0.012910	0.001766
$-0.95\beta_1$	0.927971	0.986333	0.975414	0.943112	0.935392	0.708972
β_1	0.970143	1.000969	1.016707	1.012676	1.079214	1.088831
$+0.95\beta_1$	1.012416	1.033054	1.057799	1.082239	1.223035	1.468690

Table (12): 95% confidence intervals on the regression intercept (β_o) and slope (β_1) for the 80-probe rake data at 0° clocking angles.

Coeff.	PR80	F1/2	F2/2	F3/2	F4/2	F5/2
$-0.95\beta_0$	N/A	-0.000110	-0.000677	0.000939	0.000597	0.000578
β_0	0.028025	0.000091	0.000374	0.001616	0.000971	0.000778
$+0.95\beta_0$	N/A	0.000291	0.001426	0.002293	0.001344	0.000979
$-0.95\beta_1$	0.932126	0.890575	0.841212	0.832072	0.796555	0.691544
β_1	0.970860	0.910439	0.894884	0.884288	0.852597	0.774013
$+0.95\beta_1$	1.009602	0.922820	0.948556	0.936505	0.908640	0.856481

Table (13): 95% confidence intervals on the regression intercept (β_o) and slope (β_1), 80-probe mean rake data from 10 clocking angles.

Rake	Comments	$S_{y.x}$ (F1/2)	$S_{y.x}$ (F2/2)	$S_{y.x}$ (F3/2)	$S_{y.x}$ (F4/2)	$S_{y.x}$ (F5/2)
40-probe	0° Clocking Angle	0.00298	0.00233	0.00238	0.00158	0.00647
	10 Clocking Angles	0.00051	0.00075	0.00075	0.00015	0.00674
60-probe	0° Clocking Angle	0.00009	0.00081	0.00171	0.00247	0.00176
	10 Clocking Angles	0.00003	0.00017	0.00017	0.00039	0.00073
80-probe	0° Clocking Angle	0.00045	0.00035	0.00089	0.00094	0.00121
	10 Clocking Angles	0.00024	0.00035	0.00089	0.00037	0.00026

Table (14): Summary of RMS error for each Fourier 1/2 harmonic amplitudes.

REPORT DOCUMENTATION PAGE

Form Approved
OMB No. 0704-0188

Public reporting burden for this collection of information is estimated to average 1 hour per response, including the time for reviewing instructions, searching existing data sources, gathering and maintaining the data needed, and completing and reviewing the collection of information. Send comments regarding this burden estimate or any other aspect of this collection of information, including suggestions for reducing this burden, to Washington Headquarters Services, Directorate for Information Operations and Reports, 1215 Jefferson Davis Highway, Suite 1204, Arlington, VA 22202-4302, and to the Office of Management and Budget, Paperwork Reduction Project (0704-0188), Washington, DC 20503.

1. AGENCY USE ONLY (*Leave blank*)

2. REPORT DATE
March 2002

3. REPORT TYPE AND DATES COVERED
Technical Memorandum

4. TITLE AND SUBTITLE
Considerations in the Measurement of Inlet Distortion for High Cycle Fatigue in Compact Inlet Diffusers

5. FUNDING NUMBERS
WU–708–53–13–00

6. AUTHOR(S)
Bernhard H. Anderson and Dennis J. Keller

7. PERFORMING ORGANIZATION NAME(S) AND ADDRESS(ES)
National Aeronautics and Space Administration
John H. Glenn Research Center at Lewis Field
Cleveland, Ohio 44135–3191

8. PERFORMING ORGANIZATION REPORT NUMBER
E–13243

9. SPONSORING/MONITORING AGENCY NAME(S) AND ADDRESS(ES)
National Aeronautics and Space Administration
Washington, DC 20546–0001

10. SPONSORING/MONITORING AGENCY REPORT NUMBER
NASA TM—2002-211476

11. SUPPLEMENTARY NOTES
Bernhard H. Anderson, NASA Glenn Research Center, Cleveland, Ohio, and Dennis J. Keller, RealWorld Quality Systems, Cleveland, Ohio 44116. Responsible person, Bernhard H. Anderson, organization code 5850, 216–433–5822.

12a. DISTRIBUTION/AVAILABILITY STATEMENT
Unclassified - Unlimited
Subject Category: 07 Distribution: Nonstandard
Available electronically at http://gltrs.grc.nasa.gov/GLTRS
This publication is available from the NASA Center for AeroSpace Information, 301–621–0390.

12b. DISTRIBUTION CODE

13. ABSTRACT ***(Maximum 200 words)***

It is the purpose of this study to examine the effects of engine face rake geometry (i.e., number of rake arms) and its use (i.e., with and without clocking) on the estimation of the first five Fourier harmonic 1/2 amplitudes of engine face distortion over a varied and significant set of cases. By combining the concepts of CFD analysis and Design of Experiments methodologies, a varied set of cases can be defined and analyzed which represent a large range of distortion patterns for a particular application. From the information gathered from this methodology, a rake geometry for use in Wind Tunnel tests can reasonably be defined which accurately measures the amplitudes at the "# per rev" frequencies of interest. Large reductions in both random and systematic measurement errors can be realized by clocking the engine face rake. In general, the kind of survey rake that is chosen for a Wind Tunnel experiment and the rake methodology used in providing the total pressure data needed to estimate the Fourier harmonic 1/2 amplitudes depends on the researcher's objectives and the magnitude of errors that are acceptable within the stated goals. As the need for more precise and accurate estimates of the Fourier harmonic 1/2 amplitudes increases, so does the cost of the experiment, both in researcher's time and facility time.

14. SUBJECT TERMS
Aeronautics; Propulsion; Fluid dynamics

15. NUMBER OF PAGES
37

16. PRICE CODE

17. SECURITY CLASSIFICATION OF REPORT
Unclassified

18. SECURITY CLASSIFICATION OF THIS PAGE
Unclassified

19. SECURITY CLASSIFICATION OF ABSTRACT
Unclassified

20. LIMITATION OF ABSTRACT